Binding of EBP50 to Nox organizing subunit p47^{phox} is pivotal to cellular reactive species generation and altered vascular phenotype

Imad Al Ghouleh[a,b,c], Daniel N. Meijles[b,c], Stephanie Mutchler[b,c], Qiangmin Zhang[c], Sanghamitra Sahoo[b,c], Anastasia Gorelova[b,c], Jefferson Henrich Amaral[b,c], Andrés I. Rodríguez[d,1], Tatyana Mamonova[c], Gyun Jee Song[c,e], Alessandro Bisello[c], Peter A. Friedman[c,f,g], M. Eugenia Cifuentes-Pagano[b,c], and Patrick J. Pagano[b,c,2]

[a]Division of Cardiology, Department of Medicine, University of Pittsburgh School of Medicine, Pittsburgh, PA 15213; [b]Pittsburgh Heart, Lung, Blood and Vascular Medicine Institute, University of Pittsburgh School of Medicine Pittsburgh, PA 15260; [c]Department of Pharmacology and Chemical Biology, University of Pittsburgh School of Medicine, Pittsburgh, PA 15260; [d]Heart Institute, University of São Paulo School of Medicine, Brazil; [e]Brain Science and Engineering Institute, Department of Pharmacology, School of Medicine, Kyungpook National University, Daegu 41944, Korea; [f]Laboratory for GPCR Biology, Department of Pharmacology and Chemical Biology, University of Pittsburgh School of Medicine, Pittsburgh, PA 15260; and [g]Department of Structural Biology, University of Pittsburgh School of Medicine, Pittsburgh, PA 15260

Edited by Louis J. Ignarro, University of California, Los Angeles School of Medicine, Beverly Hills, CA, and approved June 1, 2016 (received for review July 20, 2015)

Despite numerous reports implicating NADPH oxidases (Nox) in the pathogenesis of many diseases, precise regulation of this family of professional reactive oxygen species (ROS) producers remains unclear. A unique member of this family, Nox1 oxidase, functions as either a canonical or hybrid system using Nox organizing subunit 1 (NoxO1) or p47^{phox}, respectively, the latter of which is functional in vascular smooth muscle cells (VSMC). In this manuscript, we identify critical requirement of ezrin-radixin-moesin-binding phosphoprotein 50 (EBP50; aka NHERF1) for Nox1 activation and downstream responses. Superoxide ($O_2^{\bullet-}$) production induced by angiotensin II (AngII) was absent in mouse EBP50 KO VSMC vs. WT. Moreover, ex vivo incubation of aortas with AngII showed a significant increase in $O_2^{\bullet-}$ in WT but not EBP50 or Nox1 nulls. Similarly, lipopolysaccharide (LPS)-induced oxidative stress was attenuated in femoral arteries from EBP50 KO vs. WT. In silico analyses confirmed by confocal microscopy, immunoprecipitation, proximity ligation assay, FRET, and gain-/loss-of-function mutagenesis revealed binding of EBP50, via its PDZ domains, to a specific motif in p47^{phox}. Functional studies revealed AngII-induced hypertrophy was absent in EBP50 KOs, and in VSMC overexpressing EBP50, Nox1 gene silencing abolished VSMC hypertrophy. Finally, ex vivo measurement of lumen diameter in mouse resistance arteries exhibited attenuated AngII-induced vasoconstriction in EBP50 KO vs. WT. Taken together, our data identify EBP50 as a previously unidentified regulator of Nox1 and support that it promotes Nox1 activity by binding p47^{phox}. This interaction is pivotal for agonist-induced smooth muscle ROS, hypertrophy, and vasoconstriction and has implications for ROS-mediated physiological and pathophysiological processes.

NADPH oxidase | EBP50 | smooth muscle | hypertrophy | vascular tone

Reactive oxygen species (ROS) and their cellular sources have been the focus of intense study in physiology and disease for more than half a century. Under physiological conditions, ROS participate in key signaling pathways leading to distinct phenotypes including those characterized by cell migration, proliferation, differentiation, tissue remodeling, and apoptosis (1–3). Additionally, ROS mediate cell and tissue oxidative stress and damage at supraphysiological levels (2, 4, 5). The family of NADPH oxidase proteins (Nox) is widely recognized as one of the most robust and critical sources of the ROS superoxide anion ($O_2^{\bullet-}$) (2, 4). Of the 7 Nox isoforms, the Nox1 oxidase is unique in that it comes in two varieties, a canonical and a hybrid system. Canonical Nox1 is composed of Nox1, p22^{phox}, Nox organizing subunit 1 (NoxO1), Nox activating subunit 1 (NoxA1), and the small GTPase Rac1 (2). The hybrid Nox1 system employs the classical organizing subunit p47^{phox} in lieu of its more recently discovered counterpart NoxO1(6–9). Phosphorylation of p47^{phox} confers inducibility to the hybrid Nox1 oxidase, in contrast to the constitutively active canonical Nox1 oxidase (2, 6, 7, 9). Nox1 participates in the many vascular pathologies throughout the body including neointimal formation, smooth muscle hypertrophy, and vascular inflammation, among others (4, 9). However, it is currently unknown how selection for canonical- vs. hybrid-derived ROS occurs at the cellular level. It also remains elusive whether additional modulators of Nox enzymes exist. Thus, a more thorough investigation of factors that regulate Nox1 activity is critical to our fundamental understanding of the complex orchestration of events controlling oxidase function. Such knowledge is also expected to find utility in the development of therapeutics targeting ROS in disease.

Ezrin-radixin-moesin (ERM) binding phosphoprotein 50 (EBP50; aka NHERF1) is a widely expressed PDZ domain-containing scaffolding protein that associates with the actin cytoskeleton and plasma membrane by virtue of its binding to the ERM family of proteins (10–14). Recently, Bisello and coworkers (15–17) showed that EBP50 plays a role in neointimal hyperplasia and

Significance

Our findings identify a previously unidentified role for scaffolding protein ezrin-radixin-moesin-binding phosphoprotein 50 (EBP50; aka NHERF1) in the activation of NADPH oxidases (Nox), a family of professional reactive oxygen species (ROS) producing enzymes implicated in numerous pathologies. We demonstrate that EBP50 is critical for agonist-induced production of ROS superoxide anion ($O_2^{\bullet-}$), and that it directly associates with the Nox organizing subunit p47^{phox}. EBP50 deletion abolishes angiotensin II-induced cellular hypertrophy and resistance artery vasoconstriction. Given the wide array of EBP50 cellular interactions and the ubiquity of Nox, the current findings support a broader, more complex orchestration of Nox regulation than is currently hypothesized. The findings could augment future strategies targeting this interaction in disease involving aberrant ROS, tissue remodeling, and/or smooth muscle constriction.

Author contributions: I.A.G. and P.J.P. designed research; I.A.G., D.N.M., S.M., Q.Z., S.S., A.G., and A.I.R. performed research; J.H.A., G.J.S., A.B., P.A.F., and M.E.C.-P. contributed new reagents/analytic tools; I.A.G., D.N.M., and T.M. analyzed data; and I.A.G. and P.J.P. wrote the paper.

The authors declare no conflict of interest.

This article is a PNAS Direct Submission.

[1]Present address: Department of Basics Sciences, Faculty of Sciences, University of Bio-Bio, Chillan 3800708, Chile.

[2]To whom correspondence should be addressed. Email: pagano@pitt.edu.

This article contains supporting information online at www.pnas.org/lookup/suppl/doi:10.1073/pnas.1514161113/-/DCSupplemental.

contributes to vascular smooth muscle cell (VSMC) phenotype changes. Coincidentally, recent reports have implicated the Nox1 system in these responses (18, 19), therefore suggesting a potential link between EBP50 and Nox1.

Herein, we examine a previously unidentified role for EBP50 in agonist-induced activation of Nox1 and assess its effect on Nox1-mediated VSMC hypertrophy and in vivo oxidative stress. Our data support that EBP50 facilitates Nox1-derived $O_2^{\bullet-}$ production and reveal that its permissive function occurs via its binding to $p47^{phox}$. The data also show that EBP50 plays a significant role in the promotion of angiotensin II (AngII)-induced VSMC hypertrophy and resistance artery vasoconstriction.

Results

AngII- and H_2O_2-Induced $O_2^{\bullet-}$ Production Is Attenuated in VSMC from EBP50 KO Mice. Rodent VSMC express oxidase isoforms Nox1 and 4 (2, 8). We recently reported that H_2O_2, in addition to AngII, is an efficacious activator of Nox1-derived $O_2^{\bullet-}$ production in

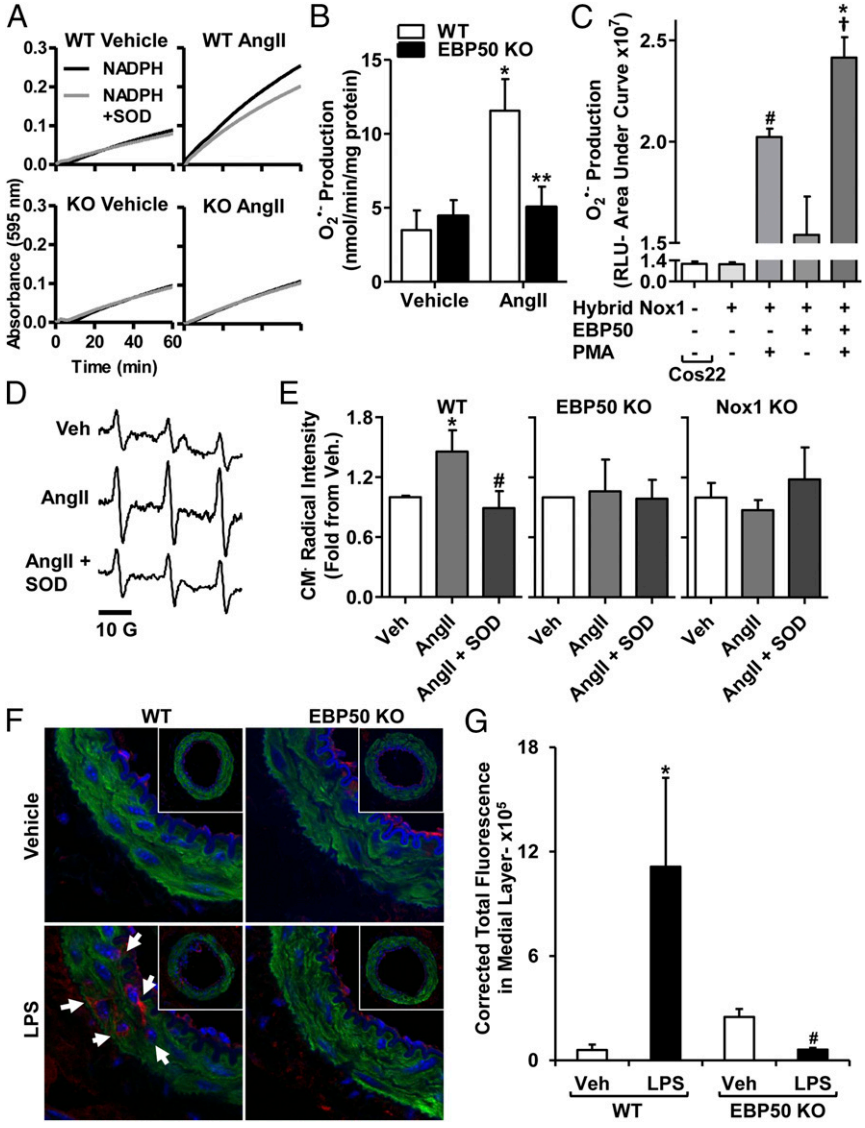

Fig. 1. EBP50 is involved in agonist-induced $O_2^{\bullet-}$ production. Representative cytochrome *c* reduction plots in the presence or absence of SOD (*A*) and bar graphs showing summary data of cytochrome *c* reduction assays (*B*) performed on 28,000 × *g* membrane fractions prepared from lysates of WT or EBP50 KO VSMC treated with 100 nM AngII. AngII induced a significant increase in $O_2^{\bullet-}$ production in WT, which was absent in EBP50 KO VSMC. Rate of $O_2^{\bullet-}$ production was quantified in $nmol \cdot min^{-1} \cdot mg^{-1}$ protein, and data are shown in *B* as means ± SEM, $n = 6–13$, $^*P < 0.01$ vs. WT vehicle; $^{**}P < 0.01$ vs. WT AngII. (*C*) L-012 assay on Cos22 cells stably expressing $p22^{phox}$ transfected with other components of the hybrid Nox1 system (Nox1, NoxA1, and $p47^{phox}$) or the hybrid Nox1 system plus EBP50 and treated with vehicle or 5 μM PMA. Data demonstrate that EBP50 augments PMA-induced $O_2^{\bullet-}$ production by the hybrid Nox1 oxidase system in Cos22 cells. White bar represents basal $O_2^{\bullet-}$ production in Cos22 cells. Data are shown as means ± SEM, $n = 24$, $^{\#}P < 0.001$ vs. vehicle-treated hybrid Nox1; $^{\dagger}P < 0.001$ vs. vehicle-treated hybrid Nox1 + EBP50; $^*P < 0.05$ vs. PMA-treated hybrid Nox1. EPR sample spectra from mouse WT aortic rings (*D*) and quantification of EPR signal amplitude (*E*) from WT, EBP50 KO, or Nox1 KO mice aortic rings subjected to vehicle or AngII (100 nM) incubation in the presence or absence of SOD (200 U/mL) using the spin probe CMH (500 μM). AngII significantly increased CM•-radical intensity (indicative of $O_2^{\bullet-}$ production) that was inhibited by SOD. This increase was absent in EBP50 KO and Nox1 KO rings. Data are shown as means ± SEM, $n = 5$, $^*P < 0.05$ vs. vehicle; $^{\#}P < 0.05$ vs. AngII. (*F*) Representative confocal images of femoral artery tissue cross-sections from LPS- or vehicle-treated WT or EBP50 KO mice stained with 4-HNE antibody (red), phalloidin (F-actin; green), and Hoechst (nuclei; blue). Autofluorescence of the internal and external elastic laminae is shown in blue. Arrows indicate locations of 4-HNE–positive fluorescence within the medial layer. (*G*) Quantification of 4-HNE fluorescence in the medial layer of femoral arteries in *A* shows that LPS induces a significant increase in tissue oxidation in WT but not EBP50 KO arteries. Data are shown as means ± SEM of corrected total fluorescence values, $n = 3–4$ animals, $^*P < 0.05$ vs. vehicle WT; $^{\#}P < 0.05$ vs. LPS WT.

VSMC (8). To assess the role of scaffolding protein EBP50 in Nox1 activation, $O_2^{\bullet-}$ production was investigated in aortic VSMC from EBP50 KO vs. WT mice. It is well established that 100 nM AngII treatment significantly increases $O_2^{\bullet-}$ levels, and this increase is Nox1-derived (20–26). We corroborated these findings using concentration and time response experiments and by showing that siRNA against Nox1 abolished the signal (Fig. S1 *A*–*C*). Thus, 100 nM AngII exposure for 4 h was selected for the current study to capture posttranslational and transcriptional Nox-derived $O_2^{\bullet-}$ production. Treatment of WT cells for 4 h with 100 nM AngII or for 1 h with 50 μM H_2O_2 resulted in a significant increase in $O_2^{\bullet-}$ measured by cytochrome *c* reduction (11.56 ± 2.14 and 11.92 ± 2.07 vs. 3.49 ± 1.33 nmol $O_2^{\bullet-}\cdot min^{-1}\cdot mg^{-1}$ membrane fraction protein for AngII- and H_2O_2- vs. vehicle-treated WT cells, respectively; Fig. 1 *A* and *B* and Fig. S2 *A* and *B*). This increase in $O_2^{\bullet-}$ was almost completely absent in EBP50 KO cells stimulated with AngII or H_2O_2 (5.04 ± 1.39 and 3.97 ± 1.34 vs. 4.44 ± 1.08 nmol $O_2^{\bullet-}\cdot min^{-1}\cdot mg^{-1}$ protein for AngII- and H_2O_2- vs. vehicle-treated KO cells, respectively; Fig. 1 *A* and *B* and Fig. S2*A*). These findings were then confirmed in VSMCs in which EBP50 was gene-silenced by stable transfection with EBP50 shRNA (Fig. S2*B*) (17). Cells stably expressing EBP50 shRNA-encoding plasmids or control GFP plasmids were treated with 50 μM H_2O_2 or vehicle for 1 h, and $O_2^{\bullet-}$ was measured. Treatment of control cells with H_2O_2 resulted in doubling $O_2^{\bullet-}$ levels compared with vehicle-treated cells, an induction abolished in EBP50 shRNA-expressing cells (Fig. S2*B*). Treatment of both groups with superoxide dismutase (SOD) completely inhibited the signal, confirming the identity of the ROS detected as $O_2^{\bullet-}$.

To investigate whether cellular EBP50 expression facilitates hybrid Nox1 activation (prevalent in VSMC), we recapitulated both EBP50 and the oxidase in Cos7 cells by transient transfection. Fig. 1*C* shows that a classical Nox activator, phorbol ester (PMA), resulted in significantly higher $O_2^{\bullet-}$ compared with vehicle-treated Nox1-transfected cells as well as untransfected cells (2.0 ± 0.05 vs. 1.1 ± 0.14 and 1.2 ± 0.16 × 10^7 RLU, respectively). PMA also increased $O_2^{\bullet-}$ in the Nox1 + EBP50 group. The increase in $O_2^{\bullet-}$ was greater in cells transfected with Nox1 + EBP50 vs. Nox1 alone (2.4 ± 0.10 vs. 2.0 ± 0.05 × 10^7 RLU). There appeared to be a rise in $O_2^{\bullet-}$ in cells transfected with both EBP50 and the hybrid Nox1 in the absence of PMA stimulation (1.5 ± 0.19 × 10^7 vs. 1.1 ± 0.14 × 10^7 RLU for vehicle-treated Nox1-transfected cells). This, however, did not reach statistical significance.

We next tested whether this observation is unique to the Nox1 hybrid system. First, Cos7 cells expressing the canonical Nox2 system (CosPhox cells) were tested for enhanced ROS production following EBP50 overexpression (CosPhox + EBP50). Fig. S3*A* demonstrates that PMA treatment results in a robust production of $O_2^{\bullet-}$ that is inhibited by diphenylene iodonium (DPI), a flavoprotein enzyme inhibitor that inhibits Nox proteins. Overexpression of EBP50 in these cells did not enhance the $O_2^{\bullet-}$ signal (Fig. S3*A*). Second, to test the canonical Nox1 system, using NoxO1, the constitutively active homolog of $p47^{phox}$, Cos7 cells were transfected with the canonical Nox1 system in the absence (CosNox1) or the presence of EBP50 overexpression (CosNox1 + EBP50). Expressing the canonical Nox1 system in Cos22 cells caused a robust, DPI-inhibitable increase in $O_2^{\bullet-}$ (Fig. S3*B*). The presence of EBP50, however, did not enhance $O_2^{\bullet-}$ production by the canonical Nox1 system (Fig. S3*B*). Taken together, these data support a unique role for EBP50 on the hybrid Nox1 system using $p47^{phox}$ as its organizing subunit.

To test whether EBP50 is essential for tissue ROS production, fresh aortic rings isolated from WT and EBP50 KO mice were incubated ex vivo with AngII in the presence or absence of SOD and subjected to electron paramagnetic resonance (EPR) and the spin trap CMH. As seen in Fig. 1 *D* and *E*, AngII induced a significant, SOD-inhibitable signal, indicative of an increase in extracellular $O_2^{\bullet-}$ production compared with vehicle. This induction was completely absent in aortas isolated from EBP50 KO mice, supporting that this protein is essential for $O_2^{\bullet-}$ generation in intact tissue. Moreover, when aortic rings from Nox1 KO mice were incubated with AngII, elevation in $O_2^{\bullet-}$ was not observed (Fig. 1 *D* and *E* and Fig. S4). These findings support a link between EBP50 and Nox1 that is essential for AngII-induced ROS. To explore whether EBP50-dependent ROS production is functional in the arterial media composed of VSMC, we contrasted tissue oxidation in femoral arteries from WT and EBP50 KO mice. Mice were subjected to vehicle or lipopolysaccharide (LPS) (10 $mg\cdot kg^{-1}$, i.p.; 16 h), another well-established activator of ROS and Nox activity (27–29), including Nox1 (30-33), the major Nox in the media of conduit arteries (1, 2, 22). Femoral arteries from these mice were isolated, sectioned, and stained for 4-hydroxynonenal (4-HNE, a footprint marker of lipid oxidation and oxidative stress). Arterial sections from LPS-treated WT animals showed significant medial 4-HNE staining (red) compared with vehicle treatment where no apparent staining was detected (Fig. 1*F*). Arteries from LPS-treated EBP50 KO mice showed no detectable 4-HNE fluorescence in the media. F-actin (phalloidin; green) and the internal and external elastic laminae (blue) demarcated the media for 4-HNE quantification. Fig. 1*G* reveals an 18-fold increase in the oxidation marker in LPS-treated WT mice vs. vehicle control (11.13 ± 5.11 vs. 0.60 ± 0.31 ×10^5 CFT units, respectively). This signal was absent in femoral arteries from LPS-treated KO mice (0.61 ± 0.11 × 10^5 CFT units).

EBP50 Regulates Nox1 Activity by Binding to $p47^{phox}$. Next, we explored a potential link between EBP50 and $p47^{phox}$. Colocalization of EBP50 and $p47^{phox}$ was investigated by confocal microscopy of rat aortic VSMC (rASMC) transfected with YFP-labeled EBP50 (green pseudocolor in the merged image) and treated with AngII. Fig. 2*A* and Fig. S5 *A* and *B* show that cells treated with vehicle followed by immunostaining for $p47^{phox}$ using Cy3-conjugated secondary antibody (red pseudocolor in the merged image and in Fig. S5*B*) revealed ubiquitous distribution of EBP50 and $p47^{phox}$ throughout the cytosol. As indicated by minimal yellow fluorescence in the merged image, EBP50 and $p47^{phox}$ display little colocalization under untreated conditions. In contrast, upon AngII treatment, increased presence of both proteins is observed, as well as enhanced presence of both proteins in or near the plasma membrane. Moreover, in the merged image, intense yellow fluorescence suggests colocalization (arrows, Fig. 2*A*). There was no autofluorescence or nonspecific secondary antibody signal in the negative control (Fig. S5*A*). To test whether there was an associated increase in expression of EBP50 and $p47^{phox}$ in addition to cellular redistribution, Western blots were performed on lysates from these cells treated with vehicle or AngII. Fig. S5*C* demonstrates that AngII treatment results in a significant increase in EBP50 protein expression. On the other hand, our data did not support a strong increase in $p47^{phox}$ expression in these cells.

To investigate whether binding between EBP50 and $p47^{phox}$ could explain their colocalization, cosedimentation experiments were performed using lysates of Cos22 cells transfected with a FLAG-tagged EBP50 and $p47^{phox}$ and stimulated with vehicle or PMA. PMA was used in these experiments because Cos7 cells do not express AngII receptors (34). Data represented in Fig. 2*B* are consistent with the association of $p47^{phox}$ and EBP50. That is, when lysates from Cos7 cells (expressing both $p47^{phox}$ and EBP50 and treated with 20 μM PMA) were immunoprecipitated with an antibody against FLAG and immunoblotted for $p47^{phox}$, a distinct band appeared consistent with the molecular weight of the organizing subunit $p47^{phox}$. Cells treated with vehicle exhibited a faint band, indicating weaker binding in the absence of stimulus.

To further explore binding of EBP50 to $p47^{phox}$, Cos7 cells were cotransfected with a CFP-$p47^{phox}$ fusion protein and

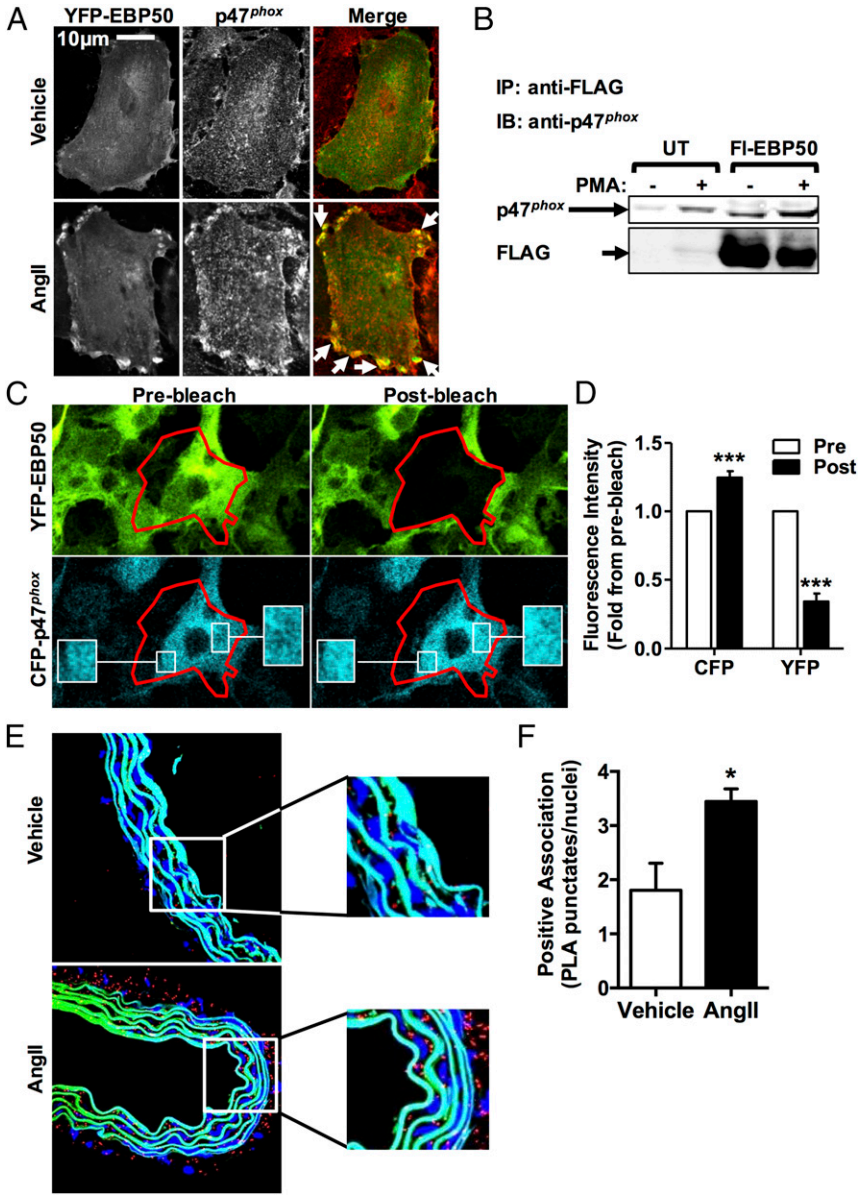

Fig. 2. EBP50 associates with p47^{phox}. (*A*) Confocal fluorescent images of VSMC transfected with YFP-labeled EBP50 (green in merge), treated with vehicle or 100 nM AngII, and stained with p47^{phox} antibody (red in merge) showing increased colocalization between EBP50 and p47^{phox} following AngII treatment. Representative of three independent experiments. Arrows indicate colocalization areas. (*B*) Immunoprecipitation with anti-FLAG antibody followed by Western blot with anti-p47^{phox} or anti-FLAG antibodies on lysates from Cos7 cells stably expressing p47^{phox} without (UT) or with FLAG-EBP50 (Fl-EBP50) transfection and treated with vehicle (–) or PMA (+). PMA treatment increases p47^{phox} association with EBP50. Representative of three independent experiments. Representative images (*C*) and fluorescence intensity quantification (*D*) of FRET experiments with confocal spectral imaging using Cos7 cells transfected simultaneously CFP-p47^{phox} and YFP-EBP50 and treated with PMA as above. Stimulation of CFP (457 nm) resulted in a YFP spectral emission (Prebleach). Acceptor (YFP) photobleaching (514 nm, 50% laser power, four cycles of 5 s) resulted in an increase in donor (CFP) fluorescence (Postbleach). These data support direct association of EBP50 and p47^{phox}. Red tracing, bleach area; white box, zoom area; Pre, prephotobleaching; Post, postphotobleacing. Data are shown as means ± SEM of fluorescence spectral emission intensity for each fluorophore, $n = 9$, $^{***}P < 0.001$ vs. prephotobleach. (*E*) Representative images of PLA experiments imaged by confocal using a 60× objective on WT mice aortic rings subjected to vehicle or AngII (100 nM) showing increased EBP50-p47^{phox} association (positive PLA; red punctates). Blue, nuclei (Hoechst); autofluorescence of the internal and external elastic laminae is shown in blue/green; white box, zoom area. (*F*) Bar graph shows quantification of punctates normalized to number of nuclei. Data and means ± SEM, $n = 3$, $^{*}P < 0.05$.

YFP-EBP50 (Fig. 2 *C* and *D*). FRET experiments with confocal spectral imaging demonstrated that fluorescent specific excitation of CFP (457 nm) resulted in spectral emission from YFP, indicating energy transfer from CFP to YFP (i.e., FRET). As can be seen in Fig. 2*C* and the fluorescence quantification in Fig. 2*D*, acceptor photobleaching of YFP-EBP50 resulted in an increase in donor CFP-p47^{phox} emission fluorescence intensity due to unquenching. FRET efficiency was calculated to be 18.99 ± 2.96%. Taken together, these results confirm a direct association between EBP50 and p47^{phox}.

Because initial experiments were performed in overexpression systems, a question remained as to whether EBP50 and p47^{phox} interacted under endogenous physiologic or pathophysiologic conditions. To test this, the proximity ligation assay (PLA), which detects tissue and cell protein–protein interaction with a resolution of 30–40 nm, was used (35). Positive proximity ligation is indicated by the appearance of punctates which localize interaction of the proteins. Fresh aortic rings isolated from WT and EBP50 KO mice were incubated ex vivo with AngII and subjected to PLA. Fig. 2 *E* and *F* demonstrate that AngII treatment resulted in an increase in PLA punctates in the aortic medial layer, indicating a direct association between EBP50 and p47^{phox} in these tissues. These data were supported by PLA experiments in rASMC cells treated with vehicle or AngII, where AngII resulted in a significant increase in punctates indicative of EBP50–p47^{phox} interaction in these cells (Fig. S6 *A*–*C*). Colocalization of endogenously expressed EBP50 and p47^{phox} corroborated these results (Fig. S6*D*). The 3D projection and serial *z*-stack visualization of AngII-treated cells confirmed membrane-proximal EBP50/p47^{phox} association and revealed cytosolic; perinuclear; and to a lesser extent, nuclear localization as well. Taken together, these data are consistent with a direct endogenous interaction between EBP50 and p47^{phox}, supporting physiological relevance.

Rho kinase 1 (ROCK1) has been indirectly linked to EBP50 because it has been shown that ERM family proteins, which associate with EBP50, are substrates of ROCK1 (11, 36). Because p47^{phox} possesses phosphorylation sites that regulate its activity, and given our present findings demonstrating p47^{phox} association with EBP50, we tested whether ROCK1 kinase associates with p47^{phox} in vascular tissues. Fresh aortic rings incubated with AngII were subjected to confocal colocalization as well as PLA. Fig. S7*A* demonstrates enhanced expression in

response to AngII of ROCK1 and p47^{phox}, in contrast to Western blot data in cells (Fig. S5*C*). No interaction between the two proteins was detected (Fig. S7 *A* and *B*).

Because EBP50 reportedly associates with its binding partners via hallmark PDZ domains (PDZ1 and PDZ2) (10, 11, 17), we searched for potential PDZ-binding motifs in p47^{phox}. Fig. 3*A* shows that a conserved PDZ-binding motif, A/T-S-A-V, exists on the C terminus of p47^{phox}. This structure falls under the class I PDZ ligands (C-terminal motif with a hydrophobic amino acid in the C-terminal residue given position number 0, any residue in position −1, a Ser/Thr in position −2, and any residue in position −3) (37–39). To model a potential interaction between this motif in p47^{phox} and a PDZ1 domain from EBP50, we used the NMR solution structure of the C-terminal tail of p47^{phox} (PDB code: 1K4U) (40) and the PDZ1 domain of EBP50 (PDB code: 1GQ4) (41). The analysis revealed that docking of the C-terminal 4 residues motif of

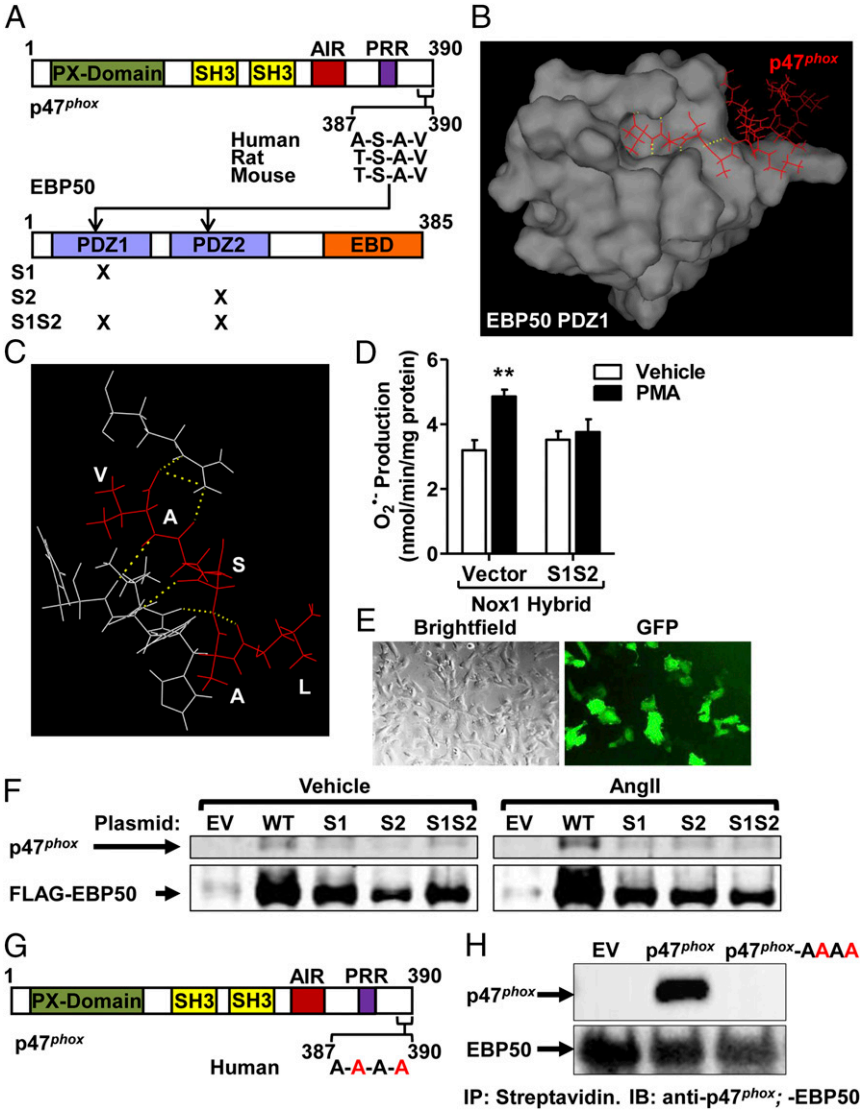

Fig. 3. The p47^{phox}-EBP50 association occurs at the PDZ domain of EBP50. (*A*) Outline of EBP50 and p47^{phox} sequence structures highlighting the PDZ domains of EBP50 and the potential PDZ-binding motif on p47^{phox}. S1, S2, and S1S2 are functional mutants of PDZ1, PDZ2, and both. (*B* and *C*) In silico dynamic modeling and docking analysis using crystal PDZ1 structure of EBP50 (PDB code 1G9O) and p47^{phox} C-terminal tail (aa 359–390; PDB code 1k4u) graphically represented using PyMol Software to show surface representation (*B*) and a magnified view of the interacting residues (*C*). Analysis reveals docking of C-terminal residues A-S-A-V of p47^{phox} in binding pocket of EBP50 PDZ1 domain and formation of hydrogen bonds. Red, p47^{phox}; white, EBP50; yellow dotted lines, hydrogen bonds. (*D*) Cytochrome *c* reduction assay on lysates of Cos22 cells transfected with Nox1 hybrid system plus empty vector or the EBP50 functional PDZ1 and 2 mutant (S1S2) and treated with vehicle or 5 μM PMA. PMA-induced $O_2^{\bullet-}$ production was abolished by expression of the functional EBP50 mutant. Rate of $O_2^{\bullet-}$ production was quantified in nmol/min/mg protein, and data are shown as means ± SEM, $n = 3$, $^{**}P < 0.01$ vs. vehicle. (*E*) Representative brightfield and GFP fluorescence images of EBP50 KO VSMC demonstrating 30–40% transfection efficiency. (*F*) Immunoprecipitation with anti-FLAG antibody followed by Western blot with anti-p47^{phox} or anti-FLAG antibodies on lysates from EBP50 KO VSMC transfected with empty vector (EV), FLAG-WT EBP50 (WT), FLAG-mutant PDZ1 EBP50 (S1), FLAG-mutant PDZ2 EBP50 (S2), or dual mutant PDZ1 and PDZ2 EBP50 (S1S2) and treated with vehicle or AngII (100 nM). AngII treatment increases p47^{phox} association with EBP50 in KO cells in which WT EBP50 was reconstituted but not in cells expressing the functional mutants of EBP50. Representative experiment. (*G*) Outline of p47^{phox} sequence structures highlighting the mutation (in red) of C-terminal PDZ-binding motif on p47^{phox}. (*H*) Immunoprecipitation with streptavidin followed by Western blot with anti-p47^{phox} or anti-EBP50 antibodies on lysates from Hek293 GnTi cells stability expressing TAP-EBP50 and transfected with empty vector (EV), WT p47^{phox} (p47^{phox}) or p47^{phox}-AAAA mutant. Interruption of the ASAV C-terminal motif of p47^{phox} disrupts its association to EBP50. Representative experiment of $n = 3$.

p47^{phox} within the ligand pocket of PDZ1 of EBP50 is favorable (Fig. 3 *B* and *C* and Fig. S8). That is, the C-terminal Val at position 0 was predicted to be buried deep within a hydrophobic pocket of PDZ1 formed by the side chains of Gly23, Tyr24, Gly25, Phe26 (GYGF loop), Leu28, Val76, and Ile79 (42, 43). Another conserved interaction typical for the class I PDZ-binding motifs is observed between the −OH group of Ser at position −2 of p47^{phox} and the imidazole group of His72 in EBP50 PDZ (42, 43). Moreover, the presence of two lysine residues at positions −5 and −7 within the C-terminal of p47^{phox}, which possess positively charged side chains, could be attracted to the negatively charged chain of Glu31 of EBP50, further stabilizing the interaction.

To verify empirically whether the interaction between EBP50 and p47^{phox} involves PDZ domains, we used mutant EBP50 plasmids lacking active PDZ1, PDZ2, or both (Fig. 3*A*). First, we tested whether PDZ interruption is associated with a reduction in ROS production. Cos7 cells were transfected with the Nox1 hybrid system in the presence or absence of the dual PDZ mutant S1S2, treated with PMA and $O_2^{\bullet-}$ production assessed by SOD-inhibitable cytochrome *c* reduction. Fig. 3*D* shows that PMA resulted in an increase in $O_2^{\bullet-}$ production that was completely absent in cells transfected with the PDZ1/2 EBP50 mutant. Next, the EBP50 mutant constructs were transfected into EBP50 KO VSMC and contrasted for p47^{phox} immunoprecipitation with WT constructs, following vehicle or AngII treatment. Transfection of GFP plasmids into these cells demonstrated an approximately 30–40% transfection efficiency as assessed by fluorescence microscopy (Fig. 3*E*). Recapitulation of WT EBP50 into EBP50 KO VSMC resulted in sedimentation of p47^{phox} as seen by coimmunoprecipitation experiments (Fig. 3*F*). This signal was increased when cells were subjected to AngII treatment. Sedimentation of p47^{phox} was markedly reduced in KO cells in which the PDZ1, PDZ2, or both mutants were transfected, both under vehicle and AngII treatment conditions. Thus, these data are consistent with a functional association of EBP50 with p47^{phox} at the PDZ domains of EBP50 that is essential for hybrid Nox1 activity.

We next tested whether the C-terminal A-S-A-V motif of human p47^{phox} is important for association with EBP50. We generated a mutant p47^{phox} in which serine 388 and valine 390 were mutated to alanine (p47^{phox}-AAAA; Fig. 3*G*). This mutant protein was contrasted to WT p47^{phox} in a heterologous system in which EBP50 was also expressed. Fig. 3*H* demonstrates that disruption of the A-S-A-V motif on p47^{phox} abolishes coimmunoprecipitation with EBP50. We observed a somewhat lower protein expression of p47^{phox}-AAAA compared with WT p47^{phox}, which could be indicative of the importance of this motif, and/or its association with EBP50, in posttranslational stability of p47^{phox} (Fig. S9 *A* and *B*).

NoxO1 in its native form lacks the A-S-A-V motif. To test whether this motif is sufficient for EBP50 interaction, we generated a NoxO1 mutant wherein the C-terminal A-S-A-V motif was appended (NoxO1-ASAV; Fig. S9*C*). WT NoxO1 displayed a weak association with EBP50 (Fig. S9*D*), likely owing to a rare and unusual potential PDZ-binding motif embedded deep within its sequence and close to the N terminus (D-T-F-V; Fig. S9*C*). In contrast, association with EBP50 was substantially augmented in cells expressing NoxO1-ASAV (Fig. S9*D*). Collectively, these data demonstrate that the A-S-A-V motif in the C-terminal of p47^{phox} is critical and sufficient for EBP50 binding.

EBP50 Is Essential for VSMC Hypertrophy. To assess whether the EBP50-modulated Nox1 leads to a change in cell phenotype, AngII-induced VSMC hypertrophy in EBP50 KO vs. WT VSMC was measured. Cells were treated with 100 nM AngII for 24 h and evaluated by FACS for the change in percentage of enlarged cells vs. vehicle controls. Treatment of WT VSMC with AngII resulted in a 30% increase in the number of enlarged cells (Fig. 4 *A* and *B*). In contrast, Fig. 4 *C* and *D* show that EBP50 KO VSMC displayed no difference in enlarged cells (vehicle vs. AngII). To confirm these findings, WT and EBP50 KO cells were treated with AngII and imaged 24 h posttreatment followed by quantification of individual cell sizes. Consistent with Fig. 4*A*, treatment of WT VSMC with AngII also resulted in a similar increase in cell size (Fig. 4 *E* and *G*). Moreover, AngII treatment of EBP50 KO VSMC resulted in no increase in cell size (Fig. 4 *F* and *H*).

To ascertain a causal link between EBP50 and Nox1, EBP50 was overexpressed (Tg-EBP50) in the presence or absence of Nox1 siRNA vs. scrambled control (8). Fig. 4*I* illustrates by FACS an approximately 100% increase in the percentage of enlarged Tg-EBP50 cells vs. untransfected controls. A similar increase was observed in Tg-EBP50, scrambled siRNA-treated cells. On the contrary, hypertrophy was significantly attenuated by cotransfection with Nox1 suppression (Fig. 4*I*). This influence of EBP50 and Nox1 was extended to modulation of AngII-induced VSMC hypertrophy. That is, FACS analysis shows ablation of the AngII response in Tg-EBP50 cells treated with Nox1 siRNA (Fig. 4*J*). These data support that EBP50, via modulation of Nox1 activity, regulates VSMC hypertrophy and has thus important implications in vascular disease.

EBP50 Is Essential for Vascular Tone Regulation of Resistance Arteries. To further extend our functional findings, we explored whether EBP50 modulates resistance vessel tone. In third-order isolated, perfused mesenteric arteries, concentration-dependent vasoconstriction in response to AngII was significantly attenuated in EBP50 KO arteries vs. WT (Fig. 5*A*). A similarly attenuated response was observed in resistance vessels from Nox1 KO mice (Fig. 5*B*). These findings were supported by data in thoracodorsal arteries (Fig. S10). The response was agonist specific because vessels from both Nox1 and EBP50 KO mice exhibited no attenuation in phenylephrine (PE)-mediated vasoconstriction relative to WT (Fig. 5 *C* and *D*).

Discussion

It is well established that Nox-derived ROS are critical components of myriad cellular pathways and drive vital responses such as host defense and inflammation. Nox-derived ROS, on the other hand, are established malefactors in aging, cancer, and neurodegenerative and cardiovascular diseases (2, 9). Despite the seminal importance of the Nox family of oxidases, little progress has been made over the past decade to delineate the mechanisms of Nox activation and regulation. This is particularly true of the Nox1 oxidase, of which two basic systems have been described (canonical vs. hybrid) and which was shown to be a central player in cardiovascular diseases (8, 9, 44, 45). In the current study we identify the scaffolding protein EBP50 as a previously unidentified binding partner and regulator of the Nox1 oxidase. We demonstrate the importance of EBP50 for ROS production in vascular cells and tissues in vitro, ex vivo, and in vivo under different stimuli and using a number of techniques. With a focus on the hybrid Nox1 system, which drives pathophysiological responses in disease, we demonstrate that EBP50, via its PDZ domains, associates with the Nox organizer subunit p47^{phox} at a unique PDZ-binding C-terminal motif. This interaction, we posit, is the means by which EBP50 regulates Nox1 activity. To investigate whether our findings carry relevance to pathophysiologic phenomena, we demonstrate, in a Nox1-associated manner, EBP50's involvement in two responses concomitant with cardiovascular disease: smooth muscle hypertrophy and resistance vessel constriction.

Initial experiments demonstrated a robust role of EBP50 in ROS production. VSMC deficient in EBP50 were incapable of producing ROS in response to AngII and H_2O_2, both potent stimuli of $O_2^{\bullet-}$ production (8, 20, 22–24, 46, 47). Ex vivo EPR studies on aortic rings also showed absence of an $O_2^{\bullet-}$ signal in response to AngII in EBP50 KO, correlating with findings in Nox1 KO. Moreover, in vivo data demonstrated that in response

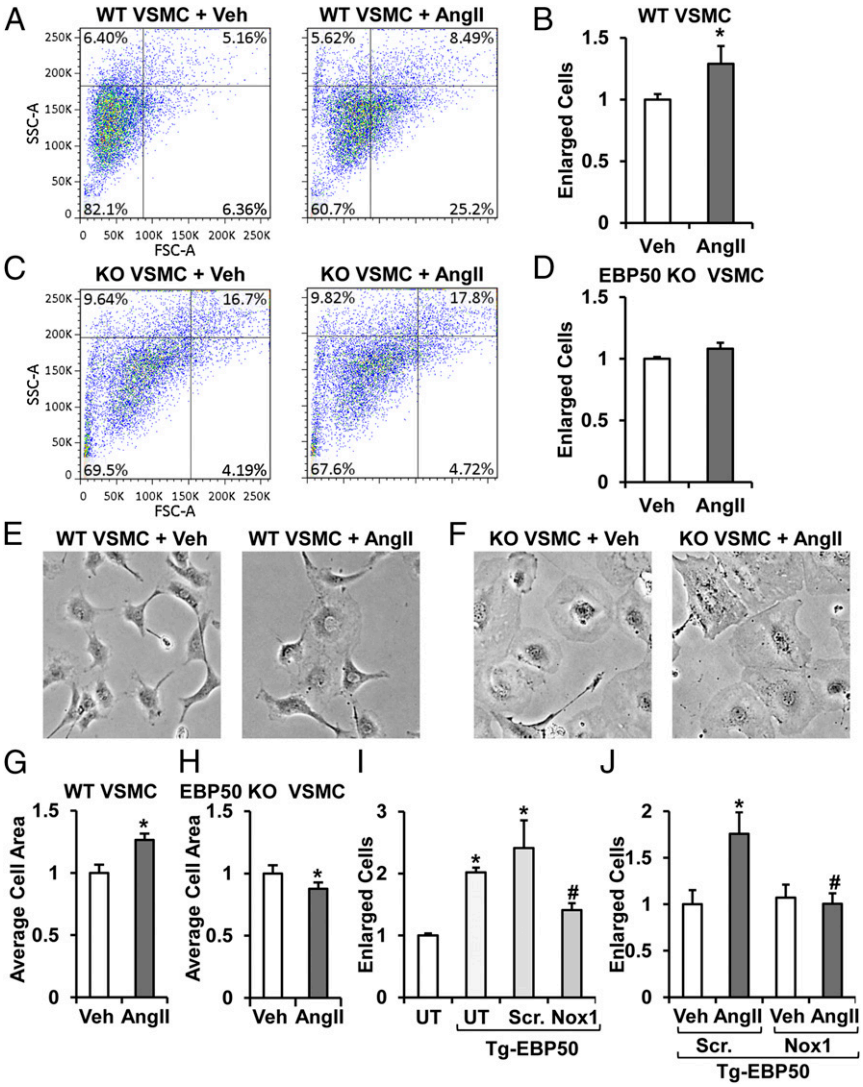

Fig. 4. AngII-induced VSMC hypertrophy is abolished in EBP50 KO cells. Representative experiment (*A* and *C*) and summary data (*B* and *D*) of FACS analysis of percent enlarged cells of total (upper right quadrant) of WT (*A* and *B*) and EBP50 KO (*C* and *D*) VSMC treated with vehicle or 100 nM AngII expressed as fold from vehicle. Data shown as means ± SEM, $n = 5–6$, $^*P < 0.05$ vs. vehicle. Representative cell images (*E* and *F*) and averaged cell size quantification expressed as fold from vehicle (*G* and *H*) of WT (*E* and *G*) and EBP50 KO (*F* and *H*) VSMC treated with vehicle or 100 nM AngII. Data are shown as means ± SEM, $n = 3$ (area of 36 cells were measured per condition from three independent experiments), $^*P < 0.05$ vs. vehicle. (*I*) FACS analysis of percent enlarged cells of total expressed as fold from untransfected control group (UT; no siRNA or Tg-EBP50) of rASMC transfected with WT EBP50 alone (UT, Tg-EBP50), WT EBP50 plus scrambled siRNA (Scr., Tg-EBP50), or WT EBP50 plus Nox1 siRNA (Nox1, Tg-EBP50). Overexpression of EBP50 significantly increased cell size in a Nox1-dependent mechanism. Data are shown as means ± SEM, $n = 3$. $^*P < 0.05$ vs. UT. $^{\#}P < 0.05$ vs. Scr. + EBP50. (*J*) FACS analysis of percent enlarged cells of total expressed as fold from scrambled siRNA vehicle-treated (Veh, Scr., Tg-EBP50) of rASMC transfected with WT EBP50 plus scrambled (Scr.) or Nox1 siRNA and treated with vehicle or 100 nM AngII. Exacerbated AngII-induced hypertrophy in EBP50 overexpressing cells was attenuated by cotransfection with Nox1 siRNA. Data are shown as means ± SEM, $n = 3$. $^*P < 0.05$ vs. Scr. + EBP50 + vehicle. $^{\#}P < 0.05$ vs. Scr. + EBP50 + AngII.

to another robust inducer of Nox-derived ROS, LPS (27–33), vascular medial smooth muscle oxidation was absent in EBP50 KO mice. Because Nox1 is a major source of $O_2^{\bullet-}$ in the vasculature, especially in VSMC (2, 8), we focused our attention on this Nox isoform. A unique hybrid Nox1 system exists in VSMC, which depends on $p47^{phox}$ as its organizer subunit in lieu of NoxO1 (6–9). Prior reports drew our attention to a possible molecular interaction between EBP50 and $p47^{phox}$. First, EBP50's interaction with actin cytoskeletal elements (11, 48, 49) piqued our interest in that $p47^{phox}$ is known to bind actin as it translocates to and activates the Nox catalytic core (2, 50–53). Moreover, the modulatory role of protein kinase C (PKC) at key sites on both molecules suggested a possible common pathway (2, 9, 54). Indeed, recapitulating the hybrid Nox1 oxidase in a heterologous Cos7 system in concert with an overexpression of EBP50 significantly augmented PMA-stimulated $O_2^{\bullet-}$ generation compared with cells basally expressing EBP50. This observation was unique to the Nox1 hybrid system because EBP50 did not enhance ROS generation by either the canonical Nox1 system or the canonical Nox2 system, which also employs $p47^{phox}$. This supports a unique role for EBP50 in regulating the hybrid Nox1 system, and it is tempting to speculate whether this occurs as a result of heretofore unknown binding partners of the EBP50–$p47^{phox}$ complex and/or a modification of $p47^{phox}$ mediated by EBP50 that channels it to Nox1 instead of Nox2.

Direct association between EBP50 and $p47^{phox}$ was demonstrated via four distinct lines of evidence. Confocal imaging experiments in VSMC confirmed that EBP50 colocalizes with $p47^{phox}$ and indicated strong membrane localization of both proteins after AngII treatment in VSMC. Coimmunoprecipitation experiments in lysates of Cos7 cells expressing both proteins

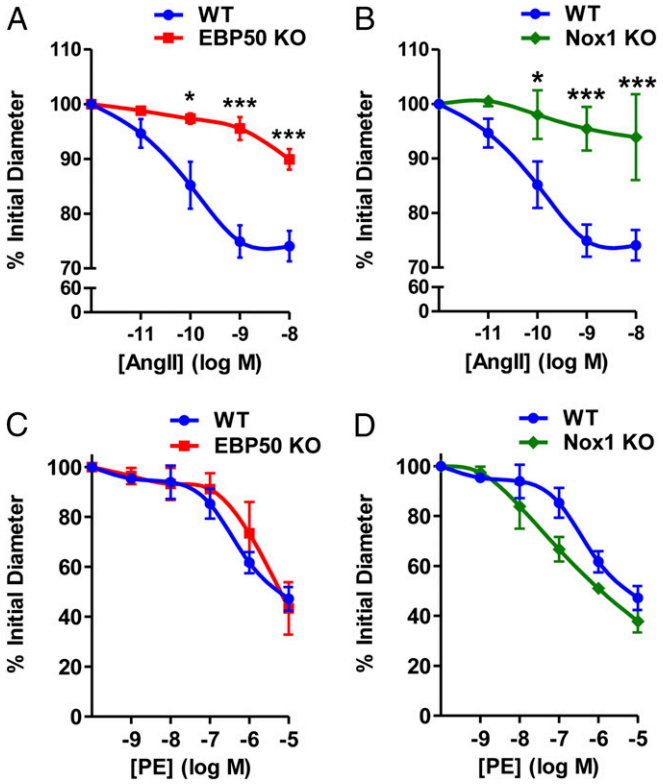

Fig. 5. EBP50 mediates resistance vessel tone. Pressure myography on isolated perfused third-order mesenteric arteries from WT and EBP50 KO (*A* and *C*) and WT and Nox1 KO (*B* and *D*) mice treated with the indicated concentrations of AngII (*A* and *B*) or phenylephrine (PE; *C* and *D*) and assessed for vasoconstriction represented as percent of initial diameter. Data shown are means ± SEM, $n = 3–5$. *$P < 0.05$ vs. WT, ***$P < 0.001$ vs. WT.

further supported a positive association that is stronger after PMA stimulation, consistent with disinhibition of p47^{phox} enhancing binding (2, 9). FRET experiments in Cos7 cells corroborate a direct association between EBP50 and p47^{phox}. Finally, PLA experiments demonstrated this binding occurs at the endogenous protein level in vascular tissues and cells.

ROCK1 has been implicated to mediate association of ERM family proteins to EBP50 by directly phosphorylating them (11). This raised the possibility that ROCK1 may interact with p47^{phox} to play a role in facilitating the latter's association with EBP50 and, henceforth, cytoskeletal elements. Our data, however, revealed that ROCK1 does not colocalize or associate with p47^{phox}. Nonetheless, ROCK may still have a yet-to-be-determined effect on components of the hybrid Nox1 system affecting their trafficking, activation, or both.

Given the protein structure of EBP50, we surmised that the interaction between EBP50 and p47^{phox} could take place on EBP50's PDZ domains. Sequence analysis of the C terminus of p47^{phox} identified a conserved potential PDZ-binding motif (A-S-A-V) and in silico docking analyses revealed that this domain can favorably dock within the hydrophobic pocket of PDZ1 domain in EBP50. Coimmunoprecipitation studies recapitulating wild-type EBP50 or functional PDZ domain mutants into EBP50 KO VSMC confirmed that EBP50's PDZ domains are critical for this interaction. Moreover, ROS detection assays showed that the PDZ domains are essential for hybrid Nox1-derived $O_2^{\bullet-}$ production. To further investigate whether the interaction involves the A-S-A-V motif in human p47^{phox}, gain-of-function/loss-of-function experiments manipulating this C-terminal A-S-A-V motif were performed. Interruption of this domain in human p47^{phox} abolished EBP50 association and addition of this domain to the C-terminal of NoxO1 substantially augmented EBP50 association. These data demonstrated that the A-S-A-V motif is both critical and sufficient for EBP50 association of p47^{phox}.

Functional significance of this interaction was deduced from smooth muscle hypertrophy and resistance vessel vasoconstriction experiments. Medial hypertrophy is causally associated with hypertension and heart failure, and Nox-derived ROS are key players in this process (55–58). In contrast to WT cells, EBP50 KO VSMC did not exhibit a hypertrophic response following treatment with AngII, a potent activator of Nox1 and inducer of VSMC hypertrophy (8, 20, 22–24, 44, 45). Overexpression of EBP50 augmented AngII-induced hypertrophy in a Nox1-dependent manner. These data demonstrate that both EBP50 and Nox1 propagate vascular hypertrophy and support a mechanism by which EBP50 regulates Nox activity leading to cellular phenotypic responses in disease.

Because vascular diseases involve both vascular tone dysfunction as well as remodeling, we investigated whether EBP50 is involved in mediating agonist-induced resistance vessel constriction. In both third-order mesenteric arteries and thoracodorsal arteries we observed a significant attenuation in AngII-induced constriction in EBP50 KO vessels. This response was virtually superimposable with the response in Nox1 KO vessels, indicative of a collaboration of the two proteins in mediating this response. The vasoconstriction response was agonist-specific because vessels from Nox1 or EBP50 KO mice exhibited a response akin to WT in response to phenylephrine. These data support that AngII and phenylephrine contractile responses diverge at the level of EBP50 and Nox1, supporting a specific ligand-receptor targeted response.

In summary, the current findings point to a mechanism of Nox regulation whereby EBP50 binds p47^{phox} and activates Nox1-derived ROS. The data support that through this binding, EBP50 promotes p47^{phox} recruitment to Nox1, bringing about oxidase assembly and activation. This interaction has functional consequences, and our results support its necessity for both medial smooth muscle hypertrophy and resistance vessel constriction. Targeting this interaction, therefore, presents a viable future therapeutic strategy to combat cardiovascular diseases. Moreover, this previously unidentified interaction has profound implications in myriad other diseases owing to the ubiquitous tissue expression of EBP50, Nox1, and p47^{phox}.

Materials and Methods

Please consult *SI Materials and Methods* for detailed methods.

Materials. A complete list of materials is provided in *SI Materials and Methods*.

Cell Culture. WT and EBP50 KO VSMC were isolated from abdominal aortas of 8- to 10-wk-old male C57BL/6 WT and KO littermates as previously described (15, 17). Rat aortic smooth muscle cells (rASMC) were purchased from Lonza Cologne GmbH. Cos7 cells stably expressing the p22^{phox} subunit (Cos22) were a kind gift from Mary C. Dinauer (Washington University School of Medicine, St. Louis, MO). Hek293 GnTi, which lack endogenous EBP50, stably expressing a TAP-domain–containing EBP50 were a kind gift from Peter Friedman (University of Pittsburgh, Pittsburgh, PA). Lentiviral shRNA expression was performed as previously described (17).

$O_2^{\bullet-}$ Detection by L-012 Chemiluminescence. L-012 (400 μM) chemiluminescence was performed as previously described (8). $O_2^{\bullet-}$ production was quantified as relative light units (RLU) area under the curve vs. time.

$O_2^{\bullet-}$ Detection by Cytochrome *c* Reduction Assay. Cytochrome *c* reduction assay was conducted as previously described (8). $O_2^{\bullet-}$ was measured in the presence of 0.2 mM cytochrome *c* and 1,000 U/mL catalase. The initial rate following NADPH (180 μM) addition of SOD-inhibitable cytochrome *c* reduction was quantified at 550 nm, and the extinction coefficient 21.1 $mmol^{-1} \bullet L\ cm^{-1}$ was used to calculate $O_2^{\bullet-}$. Because this assay measures $O_2^{\bullet-}$ in broken cells poststimulation and in the presence of the Nox substrate NADPH, it encompasses Nox activity that is due both to assembly of active

complexes as well as to removal of repression on assembled inactive complexes.

$O_2^{\bullet-}$ Detection by Electron Paramagnetic Resonance Spectroscopy. The EPR spin probe CMH (500 μM) was used to examine $O_2^{\bullet-}$ production by EPR as previously described (8, 59). Briefly, 2 mm thoracic aorta rings freshly isolated from WT, EBP50 KO, and Nox1 KO mice were treated with vehicle or AngII (100 nM, 4 h) in the presence or absence of SOD (200 U/mL). Data were quantified using the amplitude of the first spectral peak as fold from vehicle control after background subtraction.

Plasmid Transfection. Plasmids encoding full-length human cDNAs for Nox1 (pcDNA3.1-hNox1), NoxA1 (pCMVsport 6-hNoxA1), and p47^{phox} (pCMV-Tag4A-hp47) were kindly provided by David Lambeth (Emory University, Atlanta, GA). Plasmids encoding N-terminal FLAG-human WT EBP50, PDZ1 (S1), PDZ2 (S2), and PDZ1&2 (S1S2) functional mutants, as well as YFP-human WT EBP50 were a kind gift from Peter Friedman (University of Pittsburgh, Pittsburgh PA). Plasmids encoding CFP-p47^{phox} were purchased from OriGene Technologies, Inc. Site-directed mutagenesis was performed to generate the p47^{phox} serine 388 to alanine and valine 390 to alanine double mutant (p47^{phox}-AAAA). NoxO1–ASAV fusion was generated by fusing the alanine–serine–alanine–valine C-terminal motif of p47^{phox} onto the C-terminal end of NoxO1. Cos22 cells were simultaneously transfected with empty vector or plasmids for Nox1, NoxA1, and p47^{phox}; Nox1, NoxA1, p47^{phox}, and EBP50 or EBP50 S1S2 mutant; Nox1, NoxA1, and NoxO1; or Nox1, NoxA1, NoxO1, and EBP50. CosPhox cells were transfected with empty vector or EBP50. For FRET, Cos22 cells were transfected with YFP-EBP50, CFP-p47^{phox}, or YFP-EBP50 and CFP-p47^{phox}. rASMC were transfected with YFP-EBP50. For immunoprecipitation, Cos7 cells stably expressing p47^{phox} were transfected with FLAG-EBP50, and EBP50 KO VSMC were transfected with GFP control or FLAG-WT, FLAG-S1, FLAG-S2, or FLAG-S1S2 EBP50. GnTi Hek cells stably expressing TAP-EBP50 were transfected with p47^{phox}, p47^{phox} -AAAA, NoxO1, or NoxO1-ASAV.

siRNA Transfection to Suppress Nox1 in rASMC. Cells were cotransfected with EBP50 plasmid and scrambled or Nox1 siRNA (5 pmol) using Lipofectamine 2000.

Confocal 4-HNE in Vivo Immunofluorescence. C57BL/6 WT or EBP50 KO mice were injected with 10 mg·kg^{-1} i.p. LPS for 16 h. Femoral arteries were harvested, fixed, and sectioned. All animal procedures were approved by the University of Pittsburgh Institutional Animal Care and Use Committee (IACUC). Sections were incubated with anti-4-HNE antibody (Alpha Diagnostics) and Cy3-conjugated secondary antibody (Jackson ImmunoResearch) in combination with Alexa Fluor 647-conjugated phalloidin (Invitrogen). Nuclei were stained with Hoeschst dye. A total of three to four animals were used per treatment group. For each animal, three confocal images from three separate sections were captured.

Confocal in Vitro Colocalization. rASMC transfected with YFP-EBP50 on coverslips were treated with 100 nM AngII for 4 h, fixed, and permeabilized. After blocking and incubation with anti-p47^{phox} antibody and Cy3-conjugated secondary antibody, coverslips were stained with Alexa Fluor 647-phalloidin. For each experiment, five to eight confocal images per treatment group were captured. Three independent experiments were performed. No spectral overlap occurred between the different fluorescence emission channels. For endogenous protein experiments, EBP50 was assessed by an EBP50 antibody followed by Alexa Fluor 488-conjugated secondary antibody. For tissue, sections were mounted on slides, fixed, permeabilized, and blocked followed with primary antibodies for EBP50 and p47^{phox} or ROCK1 and p47^{phox} followed by secondary antibodies. Hoechst was added, and coverslips were applied.

Fluorescence Resonance Energy Transfer. Cos7 cells seeded on coverslips were transfected separately or simultaneously with CFP-p47^{phox} and YFP-EBP50, treated with PMA, and fixed. FRET experiments were performed with confocal spectral imaging using a Nikon A1 system (Nikon Instruments Inc.) as previously described with modifications (60). Emission spectra for YFP and CFP were obtained separately using spectral scanning and the excitation wavelengths of 514 or 457 nm, respectively, and used for spectral unmixing. Emission spectra on cells cotransfected with both proteins and excited with 457 nm (CFP) were unmixed. Acceptor (YFP) photobleaching was performed at 514 nm, 50% laser power, and four cycles of 5 s each. Fluorescence intensities were calculated as fold from prebleach. FRET efficiency was calculated as

$$E = \left[\left(\mathrm{CFP}_{\mathrm{post}} - \mathrm{CFP}_{\mathrm{pre}}\right)/\mathrm{CFP}_{\mathrm{pre}}\right] \times 100.$$

Proximity Ligation Assay. The proximity ligation assay (PLA) was performed according to the manufacturer's protocol (Sigma). Primary antibodies for EBP50 and p47^{phox} or p47^{phox} and ROCK1 were used. Confocal imaging was performed by capturing *z*-stacks in 10 planes for each sample and generation of maximum intensity composite *z* projections. Data were quantified as ratio of PLA punctates to number of nuclei per sample. In a subset of experiments, phalloidin was added as above. For 3D reconstruction, stacks were processed using the surface and dots features for the cell area and PLA punctates, respectively.

Immunoprecipitation and Western Blot. Cells were transfected as above. Cos7 cells were treated with vehicle or PMA (20 μM). EBP50 KO VSMC were treated with vehicle or AngII (100 nM). One hundred micrograms of cell lysates were incubated with anti-FLAG M2 resin mouse antibody overnight at 4 °C. For immunoprecipitation using Hek GnTi, cells were transfected as detailed above and lysed, and supernatants were incubated with streptavidin beads to pull down TAP-EBP50. Samples were prepared for Western blot, resolved using SDS–PAGE, and transferred onto Trans Blot nitrocellulose membranes (Bio-Rad). Membranes were blocked with the Odyssey Blocking Buffer (Li-Cor Biosciences) and incubated with primary antibodies followed by secondary antibodies (Li-Cor). Digital imaging was obtained using an Odyssey Infra-Red Imaging system (Li-Cor).

FACS Analysis for Quantification of Hypertrophy. Flow cytometry evaluation of cell hypertrophy was performed as previously described (8). Briefly, cells grown to 80% confluence and treated with vehicle or 100 nM AngII for 24 h at 37 °C were resuspended in PBS (37 °C; 1×10^6 cells per mL). Forward scatter (FSC) and side scatter (SSC) were measured recording 20,000 events per sample using a BD LSR Fortessa (BD Biosciences). Quantification was performed using FloJo (Tree Star Inc.). Density plots were gated to exclude debris and quadrant parameters were selected and assigned across all measurements based on the size of 80–85% of cells from control groups. The percentage of individual cells in quadrant 2 (FSC+, SSC+) were quantified for each group and taken as a ratio over quadrant 2 cell percentage in control groups.

Cell Size Measurement for Quantification of Hypertrophy. These experiments were carried out as previously described (8). Briefly, three to six brightfield cell images were captured (10× objective) per treatment group per experiment. The areas of four individual cells selected at random per image were quantified using Image J (NIH) and calculated as a fold from control.

Docking Analysis. In silico association analysis was performed using published crystal structures of relevant regions of p47^{phox} and EBP50: C-terminal tail of p47^{phox} (aa 359–390) complexed to C-terminal SH3 domain of p67^{phox} (PDB code: 1k4u) (40), and EBP50 PDZ1 in complex with C-terminal fragment of β2– adrenergic receptor (AR; PDB code: 1GQ4) (41), respectively. To model the C-terminal motif of p47^{phox} (LASAV sequence), the NDSLL sequence of C-terminal fragment of β2–AR was modified as follows: the C-terminal Leu^0 was replaced by Val, Leu^{-1} by Ala, Asp^{-3} by Ala, and Asn^{-4} by Leu. The generated structure includes the five residues immediately flanking the C terminus of p47^{phox} (386–390 aa) and EBP50 PDZ1 residues Leu11–Glu94. Visual modeling of predicted interaction was generated using PyMOL.

Pressure Myography. Third-order mesenteric arteries were freshly isolated from WT, EBP50 KO, and Nox1 KO mice, cannulated, pressurized (75 mm Hg), and contractile responses studied using cumulative concentrations of AngII (10^{-11} M to 10^{-7} M) or phenylephrine (PE; 10^{-9} M to 10^{-4} M). Acetylcholine (10^{-5} M) was used to verify endothelial response, and potassium chloride (40 mM) to verify vessel contraction. Maximum diameter was measured by incubating vessels in a Krebs calcium-free, ethylene glycol tetraacetic acid (EGTA, 1 mM) and sodium nitroprusside (SNP 10 μM) solution. Vessel diameter was quantified using DMT vessel acquisition software and data expressed as percent of initial diameter.

Statistical Analyses. Data are presented as means ± SEM. Data comparisons were performed with a Student's *t* test or a one- or two-way ANOVA followed by the Bonferroni post hoc analysis. Differences were deemed statistically significant at a $P < 0.05$.

ACKNOWLEDGMENTS. We thank Drs. John F. McDyer and Iulia D. Popescu for assistance in FACS protocols. We thank Dr. Guillermo Romero for critical feedback. We also thank the University of Pittsburgh Center for Biologic Imaging and Drs. Claudette M. St Croix and Simon Watkins, as well as Mark Ross, Mackenzie Mosher, and Morgan Nelson for confocal microscopy resources, assistance, and expert advice. We thank Joseph Whatley, Adam Henry, and Christina Goldbach for technical assistance. Finally, we thank Drs. Yao Li and Daniel Simoes de Jesus for assistance with some of the biochemical assays. I.A.G. received support from the American Heart Association (15SDG24910003). P.J.P. received support from the NIH (R01HL079207, R01HL112914, and P01HL103455-01). P.A.F. received support from the NIH (DK105811-01A1). Access to Center for Biologic Imaging resources was made possible in part by NIH (1S10OD019973) (S. Watkins). All Vascular Medicine Institute investigators received support from the Institute for Transfusion Medicine and the Hemophilia Center of Western Pennsylvania.

1. Lassègue B, San Martín A, Griendling KK (2012) Biochemistry, physiology, and pathophysiology of NADPH oxidases in the cardiovascular system. *Circ Res* 110(10):1364–1390.
2. Al Ghouleh I, et al. (2011) Oxidases and peroxidases in cardiovascular and lung disease: New concepts in reactive oxygen species signaling. *Free Radic Biol Med* 51(7):1271–1288.
3. Takac I, Schröder K, Brandes RP (2012) The Nox family of NADPH oxidases: Friend or foe of the vascular system? *Curr Hypertens Rep* 14(1):70–78.
4. Csányi G, Taylor WR, Pagano PJ (2009) NOX and inflammation in the vascular adventitia. *Free Radic Biol Med* 47(9):1254–1266.
5. D'Autréaux B, Toledano MB (2007) ROS as signalling molecules: Mechanisms that generate specificity in ROS homeostasis. *Nat Rev Mol Cell Biol* 8(10):813–824.
6. Bánfi B, Clark RA, Steger K, Krause KH (2003) Two novel proteins activate superoxide generation by the NADPH oxidase NOX1. *J Biol Chem* 278(6):3510–3513.
7. Brandes RP, Schröder K (2008) Composition and functions of vascular nicotinamide adenine dinucleotide phosphate oxidases. *Trends Cardiovasc Med* 18(1):15–19.
8. Al Ghouleh I, et al. (2013) Aquaporin 1, Nox1 and Ask1 mediate oxidant-induced smooth muscle cell hypertrophy. *Cardiovasc Res* 97(1):134–142.
9. Bedard K, Krause KH (2007) The NOX family of ROS-generating NADPH oxidases: physiology and pathophysiology. *Physiol Rev* 87(1):245–313.
10. Reczek D, Berryman M, Bretscher A (1997) Identification of EBP50: A PDZ-containing phosphoprotein that associates with members of the ezrin-radixin-moesin family. *J Cell Biol* 139(1):169–179.
11. Baeyens N, Horman S, Vertommen D, Rider M, Morel N (2010) Identification and functional implication of a Rho kinase-dependent moesin-EBP50 interaction in noradrenaline-stimulated artery. *Am J Physiol Cell Physiol* 299(6):C1530–C1540.
12. Naren AP, et al. (2003) A macromolecular complex of beta 2 adrenergic receptor, CFTR, and ezrin/radixin/moesin-binding phosphoprotein 50 is regulated by PKA. *Proc Natl Acad Sci USA* 100(1):342–346.
13. Troncoso M, et al. (2011) Expression of NHERF1 in colonic tumors induced by 1,2-dimethylhydrazine in rats is independent of plasma ovarian steroids. *Horm Cancer* 2(4):214–223.
14. Hayashi Y, Molina JR, Hamilton SR, Georgescu MM (2010) NHERF1/EBP50 is a new marker in colorectal cancer. *Neoplasia* 12(12):1013–1022.
15. Song GJ, et al. (2010) EBP50 inhibits the anti-mitogenic action of the parathyroid hormone type 1 receptor in vascular smooth muscle cells. *J Mol Cell Cardiol* 49(6):1012–1021.
16. Song GJ, Fiaschi-Taesch N, Bisello A (2009) Endogenous parathyroid hormone-related protein regulates the expression of PTH type 1 receptor and proliferation of vascular smooth muscle cells. *Mol Endocrinol* 23(10):1681–1690.
17. Song GJ, et al. (2012) The scaffolding protein EBP50 promotes vascular smooth muscle cell proliferation and neointima formation by regulating Skp2 and p21(cip1). *Arterioscler Thromb Vasc Biol* 32(1):33–41.
18. Lee MY, et al. (2009) Mechanisms of vascular smooth muscle NADPH oxidase 1 (Nox1) contribution to injury-induced neointimal formation. *Arterioscler Thromb Vasc Biol* 29(4):480–487.
19. Xu S, et al. (2012) Increased expression of Nox1 in neointimal smooth muscle cells promotes activation of matrix metalloproteinase-9. *J Vasc Res* 49(3):242–248.
20. Griendling KK, Minieri CA, Ollerenshaw JD, Alexander RW (1994) Angiotensin II stimulates NADH and NADPH oxidase activity in cultured vascular smooth muscle cells. *Circ Res* 74(6):1141–1148.
21. Nickenig G, et al. (2000) Negative feedback regulation of reactive oxygen species on AT1 receptor gene expression. *Br J Pharmacol* 131(4):795–803.
22. Lassègue B, et al. (2001) Novel gp91(phox) homologues in vascular smooth muscle cells: nox1 mediates angiotensin II-induced superoxide formation and redox-sensitive signaling pathways. *Circ Res* 88(9):888–894.
23. Dikalova A, et al. (2005) Nox1 overexpression potentiates angiotensin II-induced hypertension and vascular smooth muscle hypertrophy in transgenic mice. *Circulation* 112(17):2668–2676.
24. Matsuno K, et al. (2005) Nox1 is involved in angiotensin II-mediated hypertension: A study in Nox1-deficient mice. *Circulation* 112(17):2677–2685.
25. Dikalov SI, et al. (2008) Distinct roles of Nox1 and Nox4 in basal and angiotensin II-stimulated superoxide and hydrogen peroxide production. *Free Radic Biol Med* 45(9):1340–1351.
26. Basset O, et al. (2009) NADPH oxidase 1 deficiency alters caveolin phosphorylation and angiotensin II-receptor localization in vascular smooth muscle. *Antioxid Redox Signal* 11(10):2371–2384.
27. Al Ghouleh I, Magder S (2008) Nicotinamide adenine dinucleotide phosphate (reduced form) oxidase is important for LPS-induced endothelial cell activation. *Shock* 29(5):553–559.
28. Sastre E, Blanco-Rivero J, Caracuel L, Lahera V, Balfagón G (2012) Effects of lipopolysaccharide on the neuronal control of mesenteric vascular tone in rats: Mechanisms involved. *Shock* 38(3):328–334.
29. Wang XP, et al. (2011) Arginase I attenuates inflammatory cytokine secretion induced by lipopolysaccharide in vascular smooth muscle cells. *Arterioscler Thromb Vasc Biol* 31(8):1853–1860.
30. Matsuno K, et al. (2012) NOX1/NADPH oxidase is involved in endotoxin-induced cardiomyocyte apoptosis. *Free Radic Biol Med* 53(9):1718–1728.
31. Miyoshi T, et al. (2010) The role of endothelial interleukin-8/NADPH oxidase 1 axis in sepsis. *Immunology* 131(3):331–339.
32. Chéret C, et al. (2008) Neurotoxic activation of microglia is promoted by a nox1-dependent NADPH oxidase. *J Neurosci* 28(46):12039–12051.
33. Kusumoto K, et al. (2005) Ecabet sodium inhibits Helicobacter pylori lipopolysaccharide-induced activation of NADPH oxidase 1 or apoptosis of guinea pig gastric mucosal cells. *Am J Physiol Gastrointest Liver Physiol* 288(2):G300–G307.
34. Wolf G, et al. (2002) Angiotensin II activates nuclear transcription factor-kappaB through AT1 and AT2 receptors. *Kidney Int* 61(6):1986–1995.
35. Straub AC, et al. (2012) Endothelial cell expression of haemoglobin α regulates nitric oxide signalling. *Nature* 491(7424):473–477.
36. Baeyens N, de Meester C, Yerna X, Morel N (2011) EBP50 is involved in the regulation of vascular smooth muscle cell migration and cytokinesis. *J Cell Biochem* 112(9):2574–2584.
37. Harris BZ, Lim WA (2001) Mechanism and role of PDZ domains in signaling complex assembly. *J Cell Sci* 114(Pt 18):3219–3231.
38. Doyle DA, et al. (1996) Crystal structures of a complexed and peptide-free membrane protein-binding domain: Molecular basis of peptide recognition by PDZ. *Cell* 85(7):1067–1076.
39. Songyang Z, et al. (1997) Recognition of unique carboxyl-terminal motifs by distinct PDZ domains. *Science* 275(5296):73–77.
40. Kami K, Takeya R, Sumimoto H, Kohda D (2002) Diverse recognition of non-PxxP peptide ligands by the SH3 domains from p67(phox), Grb2 and Pex13p. *EMBO J* 21(16):4268–4276.
41. Karthikeyan S, Leung T, Ladias JAA (2001) Structural basis of the Na+/H+ exchanger regulatory factor PDZ1 interaction with the carboxyl-terminal region of the cystic fibrosis transmembrane conductance regulator. *J Biol Chem* 276(23):19683–19686.
42. Mamonova T, Kurnikova M, Friedman PA (2012) Structural basis for NHERF1 PDZ domain binding. *Biochemistry* 51(14):3110–3120.
43. Mamonova T, et al. (2015) Canonical and noncanonical sites determine NPT2A binding selectivity to NHERF1 PDZ1. *PLoS One* 10(6):e0129554.
44. Ushio-Fukai M, Alexander RW, Akers M, Griendling KK (1998) p38 Mitogen-activated protein kinase is a critical component of the redox-sensitive signaling pathways activated by angiotensin II. Role in vascular smooth muscle cell hypertrophy. *J Biol Chem* 273(24):15022–15029.
45. Touyz RM, Yao G, Viel E, Amiri F, Schiffrin EL (2004) Angiotensin II and endothelin-1 regulate MAP kinases through different redox-dependent mechanisms in human vascular smooth muscle cells. *J Hypertens* 22(6):1141–1149.
46. Li WG, et al. (2001) H(2)O(2)-induced O(2) production by a non-phagocytic NAD(P)H oxidase causes oxidant injury. *J Biol Chem* 276(31):29251–29256.
47. Boulden BM, et al. (2006) Early determinants of H2O2-induced endothelial dysfunction. *Free Radic Biol Med* 41(5):810–817.
48. Bretscher A, Chambers D, Nguyen R, Reczek D (2000) ERM-Merlin and EBP50 protein families in plasma membrane organization and function. *Annu Rev Cell Dev Biol* 16:113–143.
49. Voltz JW, Weinman EJ, Shenolikar S (2001) Expanding the role of NHERF, a PDZ-domain containing protein adapter, to growth regulation. *Oncogene* 20(44):6309–6314.
50. Touyz RM, Yao G, Quinn MT, Pagano PJ, Schiffrin EL (2005) p47phox associates with the cytoskeleton through cortactin in human vascular smooth muscle cells: Role in NAD(P)H oxidase regulation by angiotensin II. *Arterioscler Thromb Vasc Biol* 25(3):512–518.
51. Touyz RM, Yao G, Schiffrin EL (2005) Role of the actin cytoskeleton in angiotensin II signaling in human vascular smooth muscle cells. *Can J Physiol Pharmacol* 83(1):91–97.
52. Tamura M, Itoh K, Akita H, Takano K, Oku S (2006) Identification of an actin-binding site in p47phox an organizer protein of NADPH oxidase. *FEBS Lett* 580(1):261–267.
53. Tamura M, Kai T, Tsunawaki S, Lambeth JD, Kameda K (2000) Direct interaction of actin with p47(phox) of neutrophil NADPH oxidase. *Biochem Biophys Res Commun* 276(3):1186–1190.
54. Fouassier L, et al. (2005) Protein kinase C regulates the phosphorylation and oligomerization of ERM binding phosphoprotein 50. *Exp Cell Res* 306(1):264–273.
55. Parker SB, Wade SS, Prewitt RL (1998) Pressure mediates angiotensin II-induced arterial hypertrophy and PDGF-A expression. *Hypertension* 32(3):452–458.
56. Griffin SA, et al. (1991) Angiotensin II causes vascular hypertrophy in part by a non-pressor mechanism. *Hypertension* 17(5):626–635.
57. Kamal MF, Campbell AC (1979) Medial hypertrophy in the small intestinal arteries in systemic hypertension, renal and essential. *J Pathol* 129(2):99–110.
58. Dzau VJ, Gibbons GH (1988) Cell biology of vascular hypertrophy in systemic hypertension. *Am J Cardiol* 62(11):30G–35G.
59. Csányi G, et al. (2012) Thrombospondin-1 regulates blood flow via CD47 receptor-mediated activation of NADPH oxidase 1. *Arterioscler Thromb Vasc Biol* 32(12):2966–2973.
60. Ranayhossaini DJ, et al. (2013) Selective recapitulation of conserved and nonconserved regions of putative NOXA1 protein activation domain confers isoform-specific inhibition of Nox1 oxidase and attenuation of endothelial cell migration. *J Biol Chem* 288(51):36437–36450.
61. Price MO, et al. (2002) Creation of a genetic system for analysis of the phagocyte respiratory burst: High-level reconstitution of the NADPH oxidase in a nonhematopoietic system. *Blood* 99(8):2653–2661.